AIAA 2002-0944

Numerical Study of a Convective Turbulence Encounter

Fred H. Proctor and David W. Hamilton
NASA Langley Research Center
Hampton, VA

Roland L. Bowles
AeroTech Research, Inc.
Hampton, VA

40th Aerospace Sciences Meeting & Exhibit
14-17 January 2002 / Reno, NV

AIAA-2002-0944

NUMERICAL STUDY OF A CONVECTIVE TURBULENCE ENCOUNTER

Fred H. Proctor* and David W. Hamilton†
NASA Langley Research Center
Hampton, Virginia

Roland L. Bowles‡
AeroTech Research, Inc.
Hampton, Virginia

Abstract

A numerical simulation of a convective turbulence event is investigated and compared with observational data. The specific case was encountered during one of NASA's flight tests and was characterized by severe turbulence. The event was associated with overshooting convective turrets that contained low to moderate radar reflectivity. Model comparisons with observations are quite favorable. Turbulence hazard metrics are proposed and applied to the numerical data set. Issues such as adequate grid size are examined.

Introduction

A major portion of the accidents from aircraft turbulence encounters are within close proximity of atmospheric convection (e.g., thunderstorms).[1] The National Aeronautics and Space Administration (NASA), through its Aviation Safety Program, is testing technologies that will reduce the risk of injuries from these types of encounters. Primary focus of the turbulence element within this program is the characterization of turbulence and its environment, and the development and testing of hazard-estimation algorithms for both radar and *in situ* detection. The ultimate goal is to operationally test onboard sensors that will provide ample warning prior to encounters with hazardous turbulence. In support of turbulence characterization, numerical modeling of atmospheric convection is being conducted using a large eddy simulation model. A special need for the modeling is to provide realistic data sets for developing and testing turbulence detection sensors. However, the first step prior to this application must be verification that the numerical model can produce useful and realistic data sets. To meet this goal numerical simulations with NASA's Terminal Area Simulation System (TASS) are being applied to actual cases with moderate and severe turbulence encounters. Validation of the numerical simulations relies on measurements from radars, satellites, and aircraft penetrations.

One particular case targeted for numerical study is a turbulence event encountered during NASA's fall-2000 flight tests. In this event, hazardous turbulence was encountered by NASA Langley's B-757 on 14 December 2000. Severe intensities of turbulence were measured as the aircraft penetrated updraft plumes near the top of a narrow line of thunderstorms. Data from onboard Doppler radar, *in situ* wind and temperature measurements, and recorded NEXRAD radar data (Tallahassee (TLH)) are available for comparison with the numerical simulation of this case. This paper will describe the conditions associated with

*Research Scientist, Airborne Systems Competency, AIAA member
†Research Scientist, Airborne Systems Competency
‡Senior Research Engineer, Retired NASA

the turbulence encounter and analyze results from the simulation of this event.

Description of Event

During two test days in December 2000, regions of convective turbulence were purposefully encountered by NASA's B-757. Areas with moderate or greater radar reflectivity, i.e. RRF > 35 *dBZ*, were avoided as routinely done by commercial air carriers. Turbulence measurements from the *in situ* system were quantified in terms of RMS normal loads (σ_{ng}), where $0.20\ g \leq \sigma_{ng} \leq 0.30\ g$ is considered moderate and $\sigma_{ng} > 0.30\ g$ is severe. During two flights, 14 moderate and 4 severe turbulence encounters occurred in the vicinity of deep convection. Further details of these encounters can be found in a companion paper presented at this conference.[2]

The turbulence event selected for study was the strongest event encountered during the flight tests. This event, 191-6 (referred as 191.3 in reference [2]), had a peak turbulence intensity of σ_{ng} = 0.44 g, which is comparable to that in several incidents involving commercial aircraft (see Fig. 15 in Hamilton and Proctor[2]). The *in situ* measurements of vertical wind and RMS normal loads during this encounter are shown in Fig. 1. The turbulence was characterized by sharp oscillations in vertical velocity over a distance of about 5 *km*.

Event 191-6 was associated with a narrow line of convective cells extending east-northeast (*ENE*) from the Gulf of Mexico through the Florida Panhandle (Fig. 2). Storm tops reached 11.8 *km* (39,000 *ft*) mean sea level (MSL) with cell movement from the west-southwest (*WSW*) at about 20 *m/s*. Turbulence was encountered as the NASA B-757 flew through weak radar reflectivity regions near the top of the convective line. At the time of penetration, the aircraft was at an altitude of 10.3 *km* above ground level (AGL), and was at a location just north of the Florida-Georgia state line (latitude, longitude: -84.17 *W*, 30.76 *N*). The aircraft heading was *ENE* (nearly parallel to the line) with an air speed of about 235 *m/s*. Further details of the flight test and meteorology surrounding this event are in Hamilton and Proctor[2].

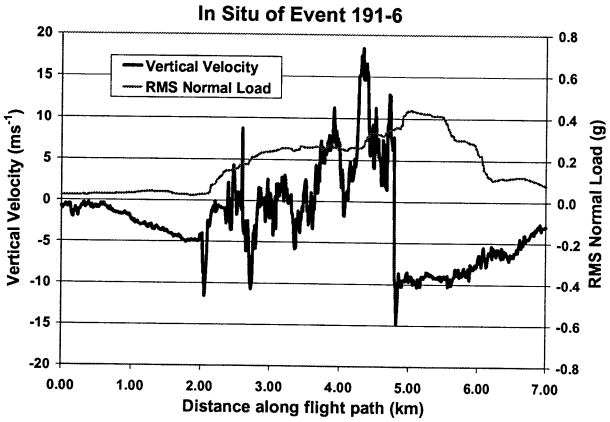

Figure 1. *Measured vertical wind and RMS normal load acceleration vs distance along the flight path during event 191-6.*

The approach taken in this paper is to perform a numerical simulation of the convective line and examine subsequent turbulence fields near the altitude of the 191-6 encounter.

The Model and Initial Conditions

The numerical simulation is carried out with the Terminal Area Simulation System[3,4] (TASS), which is a large eddy simulation model developed for simulating convective clouds and atmospheric turbulence.

Model Equations

The TASS model consists of 12 prognostic equations: three equations for momentum, one equation each for pressure deviation and potential temperature, six coupled equations for continuity of water substance (water vapor, cloud droplet water, cloud ice crystals, rain, snow and hail) and a prognostic equation for a massless tracer. The model also contains numerous microphysics models for computing cloud and precipitation physical interactions. Further details of the model formulation can be found in references [3, 5, and 6].

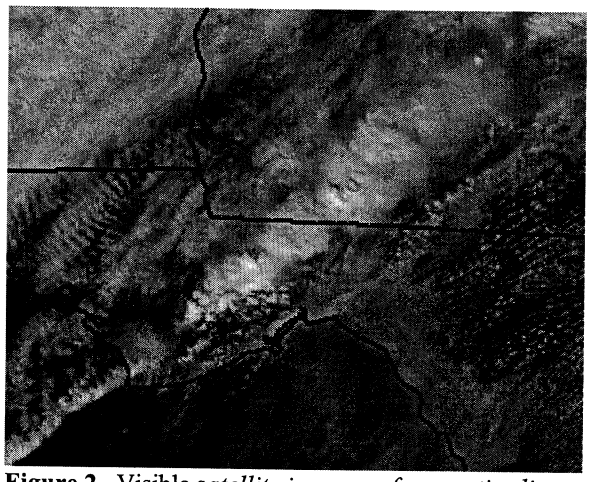

Figure 2. Visible *satellite imagery of convective line near the time of event 191-6.*

The TASS equation set (ignoring Coriolis terms) in standard tensor notation is as follows:

Momentum:

$$\frac{\partial u_i}{\partial t}+\frac{H}{\rho_o}\frac{\partial p}{\partial x_i}=-\frac{\partial u_i u_j}{\partial x_j}+u_i\frac{\partial u_j}{\partial x_j}+g\,(H-1)\delta_{i3}$$

$$+\frac{1}{\rho_o}\frac{\partial}{\partial x_j}\rho_o K_M\left[\frac{\partial u_i}{\partial x_j}+\frac{\partial u_j}{\partial x_i}-\frac{2}{3}\frac{\partial u_k}{\partial x_k}\delta_{ij}\right]$$

Buoyancy Term:

$$H=\left(\frac{\theta}{\theta_o}-\frac{p\,C_v}{P_o C_p}\right)[1+0.61(Q_v-Q_{vo})-Q_T]$$

Pressure Deviation:

$$\frac{\partial p}{\partial t}+\frac{C_p P}{C_V}\frac{\partial u_j}{\partial x_j}=\rho_o g\,u_j\delta_{j3}$$

Thermodynamic Equation (Potential Temperature):

$$\frac{\partial \theta}{\partial t}=-\frac{1}{\rho_o}\frac{\partial \theta\,\rho_o u_j}{\partial x_j}+\frac{\theta}{\rho_o}\frac{\partial \rho_o u_j}{\partial x_j}$$

$$+\frac{1}{\rho_o}\frac{\partial}{\partial x_j}[\rho_o K_H\frac{\partial \theta}{\partial x_j}]+\frac{L\theta}{T\,C_p}S$$

with the *Potential Temperature* defined as:

$$\theta=T\left(\frac{P_{oo}}{P}\right)^{\frac{R_d}{C_p}}$$

In the above equations, u_i is the tensor component of velocity, t is time, p is deviation from atmospheric pressure P, T is atmospheric temperature, ρ is the air density, C_p and C_v are the specific heats of air at constant pressure and volume, g is the earth's gravitational acceleration, R_d is the gas constant for dry air, P_{oo} is a constant equivalent to 1000 *millibars* (10^5 *pascals*) of pressure, Q_v is the mixing ratio for water vapor, Q_T is sum of the mixing ratios for liquid and ice substances, L is the latent heat, and S is a water substance source term. Environmental state variables, e.g., ρ_o, Q_{vo}, P_o, and θ_o, are defined from the initial input sounding and are functions of height only.

Conservation of Scalar Variables (e.g., water vapor, cloud droplet water, etc.):

$$\frac{\partial Q}{\partial t}=-\frac{1}{\rho_o}\frac{\partial Q\,\rho_o u_j}{\partial x_j}+\frac{Q}{\rho_o}\frac{\partial \rho_o u_j}{\partial x_j}$$

$$+\frac{1}{\rho_o}\frac{\partial}{\partial x_j}[\rho_o K_H\frac{\partial Q}{\partial x_j}]+S$$

For precipitating variables (such as rain and snow), an additional vertical flux term is added to account for fall out.

A modified Smagorinsky first-order closure is used for the subgrid eddy viscosity as:

$$K_M=l_s^2\sqrt{\frac{\partial u_i}{\partial x_j}\left(\frac{\partial u_i}{\partial x_j}+\frac{\partial u_j}{\partial x_i}\right)-\frac{2}{3}\left(\frac{\partial u_k}{\partial x_k}\right)^2}\;\bullet$$

$$\sqrt{1-\alpha_1 Ri_s-\alpha_2 Ri_r}$$

The subgrid eddy viscosity for momentum, K_M, is modified by the Richardson numbers, for stratification, Ri_s, and for flow rotation, Ri_r, with $\alpha_1 = 3$ and $\alpha_2 = 1.5$. The subgrid eddy viscosity for heat and water substance is determined as $K_H = 3K_M$. The subgrid length scale, l_s is determined from the grid volume.

Numerical Approximations

Time-derivative approximations for momentum and pressure are time-split explicit for computational efficiency. The prognostic equations are approximated using 4th-order energy-conserving space differencing and 2nd order time differencing. Only light numerical filtering is applied using a 6th-order filter. Potential temperature and water substances equations are approximated with third-order accurate time and space differences with upstream-biased quadratic interpolation.[7] The horizontal derivatives in TASS are approximated on an Arakawa-C grid.[8] The numerical formulation for TASS is stable for long-term integrations and is essentially free from numerical diffusion.[9]

Model Domain and Boundary Conditions

The domain is rotated 66° clockwise such that the x-coordinate is orthogonal to the convective line and the y-coordinate is parallel to the line (see Fig. 3). The physical size of the domain is 25 *x* 25 *x* 14 *km*. The grid size is uniform at 100 *m* over most of the domain, except below an altitude of 2000 *m* where grid stretching shrinks the vertical size to 50 *m*. The domain is resolved by 148 vertical levels having 251 x 251 grid points.

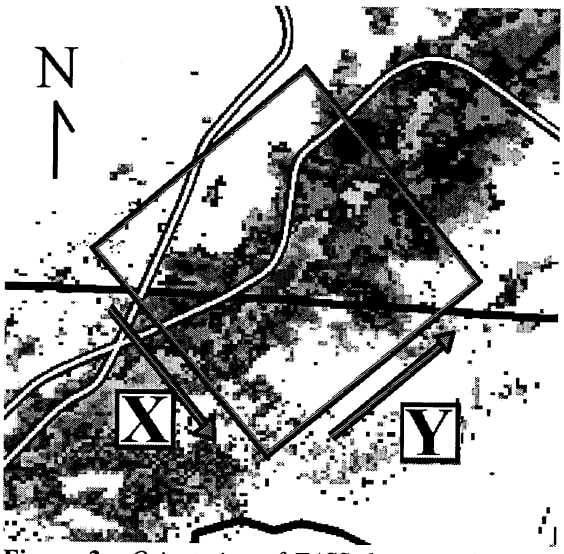

Figure 3. *Orientation of TASS domain relative to convective line. Observed composite radar reflectivity field and flight path depicted near the time of event 191-6.*

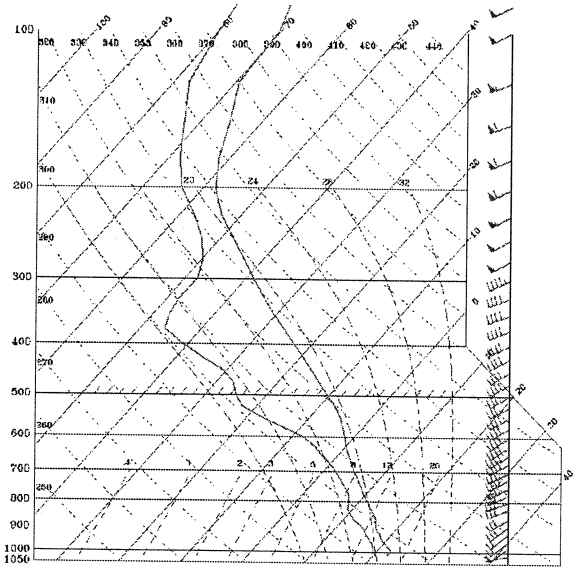

Figure 4. *Skew-T chart with atmospheric sounding for time and location near event 191-6. Generated from forecast with Mesoscale Atmospheric Simulation System. Sounding data provide by Mike Kaplan, NCSU, under NASA contract NAS1-99074.*

Periodic boundary conditions are assumed at the northeastern and southwestern boundaries (orthogonal to the convective line), while open nonreflective conditions are assumed for the northwestern and southeastern boundary.

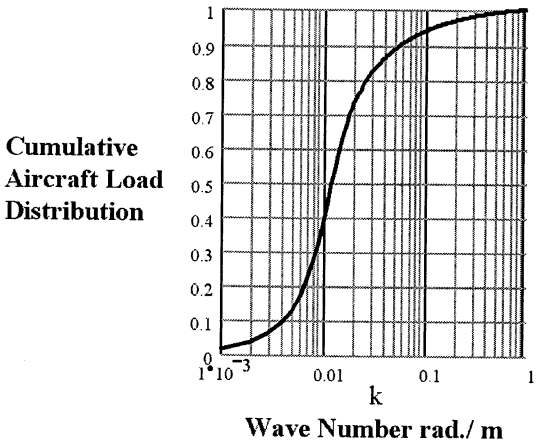

Figure 5. *Cumulative distribution of normalized aircraft loads as a function of wave number. Aircraft calculation based on B-757-200 frequency domain model at an altitude of 6.1 km with an airspeed of 212 m/s and a weight of 180,000 lbs. Assumes von Karman turbulence spectrum with an outer scale of 300 m and* $\sigma_w = 1$.

The ground boundary is impermeable with nonslip velocity specifications. The surface stress due to the ground is determined locally from the wind speed, surface roughness, and the local thermal stratification. Details of the surface formulation are in the appendix of Proctor and Han.[10]

Initial Conditions

The simulation is initialized with a vertical distribution of temperature, dew point, and wind velocity, representative of the environment near the time and location of the turbulence event. Since observed profiles were unavailable at the time and location of event 191-6, a forecast sounding (Fig. 4) was obtained from a mesoscale prediction model.[11]

Subgrid Fusion

In order to model scales of motion important for aircraft response, high resolution is needed. Results from a frequency-domain flight dynamics model,[12,13] indicated that scales of motion as small as 50 *m* (wave number of 0.126 *rad/m*) are needed in order to capture at least 97% of the cumulative aircraft load distribution (Fig. 5). Available computer capability and the size of the computations restricts the grid size to about 100 *m*. Although this resolution misses scales that are important for aircraft response, the model's ability to

simulate the larger-scale features of a convective-turbulence event can be assessed. This evaluation is discussed in the first part of the next section. High-resolution turbulence fields are achieved by extracting a subdomain from the numerical simulation and merging it with subgrid turbulence fields[14]. Results from this procedure, including onboard radar and aircraft simulations, are discussed in the second part of the next section.

Results

Simulation of Convective Line

Results from the TASS 100*m* simulation of the convective line are presented below, and are compared with observations derived from ground based NEXRAD radar and B-757 flight data. Table 1 shows comparisons between model and observations of selected features.

Table 1. Model Comparison

Variable	TASS	Observed
Orientation of Line	*WSW-ENE*	*WSW-ENE*
Peak Storm Tops	11.5 *km*	11.8 *km*
Peak Radar Reflectivity at Ground	53.5 *dBZ*	55 *dBZ*
Peak Radar Reflectivity at z=9 *km*	38.9 *dBZ*	40 *dBZ*
Cell Motion (toward)	*ENE* at 19 *m/s*	*ENE* at 17 *m/s*
Width of Convective Line near Ground Level (based on 20 *dBZ*)	6 *km*	8 *km*
Peak Eddy Dissipation Rate ($m^{2/3}/s$)	0.86	0.74
Horizontal Scale of Turbulence Patch at Flight Level	5 *km*	5-6 *km*

Comparisons between modeled radar reflectivity and that observed by the Tallahassee radar are depicted in Figs 6-9. The model values are without consideration of the radar beam width, pulse length, and beam tilt. Nevertheless, only small differences exist, and comparisons show similar orientation, scale, and magnitude.

The radar reflectivity from the onboard radar just before encountering event 191-6 is shown in Fig. 10. A simulation of this radar using the TASS data set is shown for comparison in Fig. 11. Both show similar scale and intensity, although details in the echo structure differ.

A three-dimensional perspective of the simulated convective line appears quite realistic, exhibiting cumulus turrets, anvil outflow and overshooting tops (Fig. 12). The convective cells exhibit downwind tilt (toward the northeast) with most of the anvil outflow spreading in that direction. During the actual encounter, the NASA B-757 flew toward the northeast parallel to the line and entered the overshooting cloud areas near the storm tops. Severe turbulence was encountered as the aircraft skirted the northwestern flank of the convective line.

In Fig. 13, a horizontal cross section of vertical velocity is show at the flight level of the NASA B-757. Also superimposed is the TASS radar reflectivity (truncated at 15 *dBZ*). The radar reflectivity is primarily due to the presence of snow, with temperatures at this altitude being colder than –40°*C*. Localized regions of strong upward velocity (peak of 17 *m/s*) are associated with rising convective turrets and are embedded within low-radar reflectivity regions. Strong downward motions are especially noted on the downwind side of the turrets. This feature also was observed during the flight test and is discussed in Hamilton and Proctor.[2] Radar reflectivity within the downdraft regions is weak in comparison with the updraft regions. Also note that strong gradients of vertical velocity may occur in regions where radar reflectivity is less than 20-15 *dBZ*. Similarly, the *in situ* vertical velocity derived from the B-757 (Fig. 1), also shows intense pulses of updraft and downdraft during this turbulence event.

Figure 14 shows TASS eddy-dissipation rate (EDR) for the same region as depicted in Fig. 13. Although the strongest values are located within higher reflectivity regions (i.e., greater 25 *dBZ*), moderate to strong values may occur in regions of weak radar reflectivity. As indicated in Table 1, the peak values of simulated EDR are similar to those obtained from *in situ* data of the actual encounter.

An energy spectrum computed from the TASS velocity data (Fig. 15) indicates a continuous spectra of turbulence rather than an isolated gust. This also is confirmed from spectrum of flight data that was measured during the actual event.[2] The TASS spectra (Fig. 15) appears to have an inertial subrange with a -5/3 slope especially at larger wavelengths. At smaller

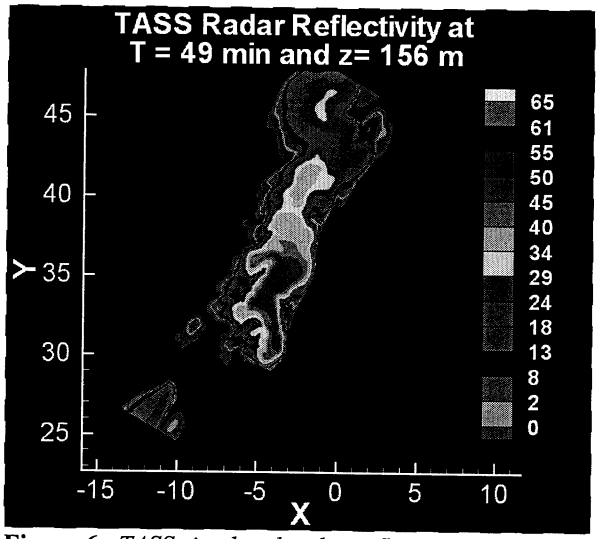

Figure 6. *TASS simulated radar reflectivity (dBZ) in horizontal plane at 156 m altitude (abscissa and ordinate have units of km).*

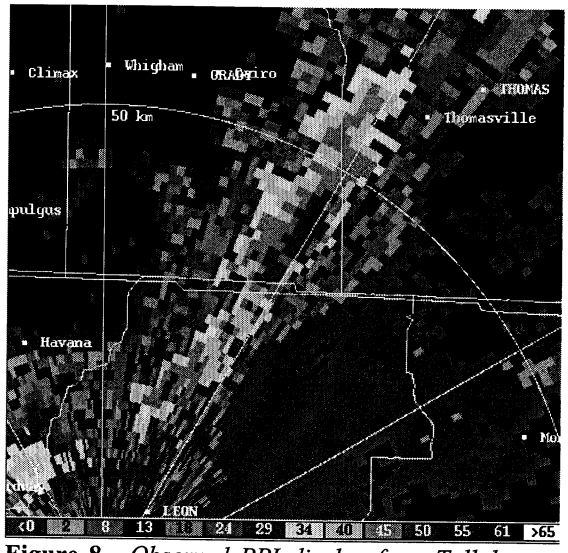

Figure 8. *Observed PPI display from Tallahassee NEXRAD radar at 1.4 degree tilt, near time of event 191-6.*

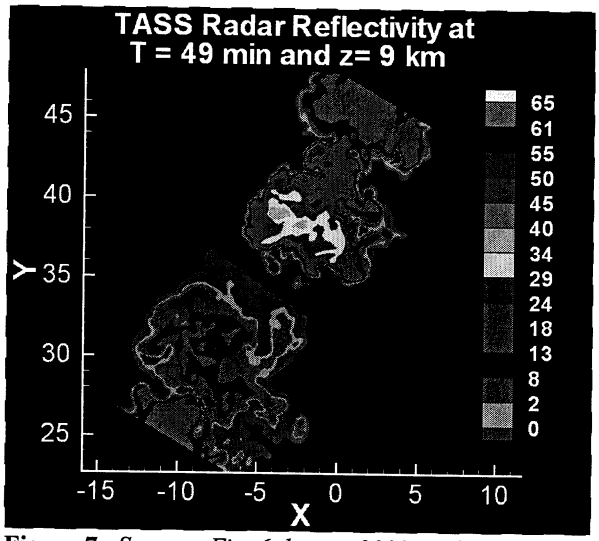

Figure 7. *Same as Fig. 6, but at 9000 m altitude.*

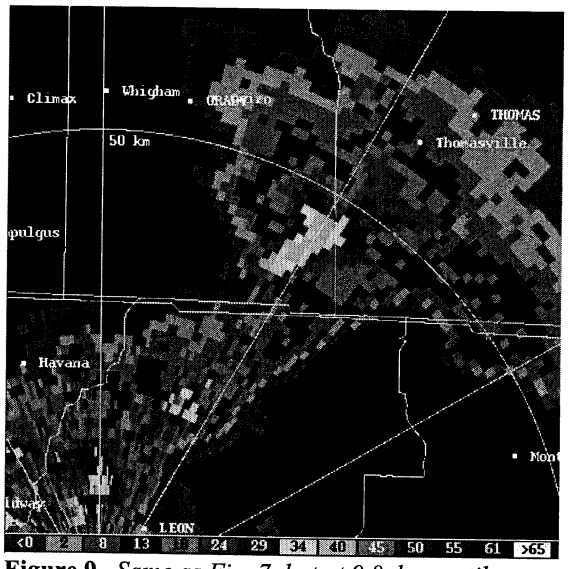

Figure 9. *Same as Fig. 7, but at 9.8 degree tilt.*

wavelengths, however, the spectra shows a steeper slope than the theoretical -5/3 slope. This drop-off in energy at higher wavenumbers is often found in other LES studies,[15,16] and is theoretically expected since values at each grid cell represent volumetric averages rather than point values.[17]

Merging with Subgrid Turbulence

Although the 100*m* TASS simulation was able to simulate the larger-scale features of the turbulence event, it could not resolve the smaller-scales of motion important for aircraft response calculations. Figure 15 shows that only wavelengths greater than 600 m (6 grid points) are adequately resolved, and according to Fig. 5 only 40% of the cumulative aircraft load is captured at these frequencies. Since finer resolution is needed for proper aircraft response simulation and turbulence radar simulation, high-resolution subgrid turbulence fields were merged with a subdomain of the TASS simulation. This data set was generated by NCAR using the following procedure:[18]

1) A sub-volume of the domain was selected which encompassed the turbulence event.

2) The variables (at t=48 min) were interpolated to a 25 *m* grid, within a 12.8 *km* x 12.8 *km* horizontal and 3.2 *km* vertical subdomain.
3) Following a technique devised by Frehlich *et al*[14], subgrid wind fields using a von Karman algorithm were then merged with the TASS data. The von Karman subgrid parameters (variance and outer length scale) were determined from a best fit of the model generated structure functions (after interpolation) to the desired Kolmogorov behavior.

Subgrid fields are only added to the velocity fields. Other fields, such as radar reflectivity are simply interpolated to the higher-resolution subdomain.

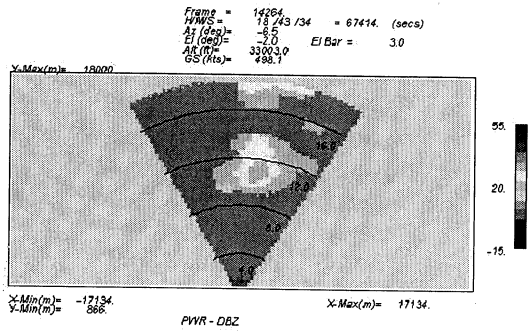

Figure 10. *Radar reflectivity (dBZ) from onboard turbulence radar. Observed just prior to encounter with event 191-6. Range rings every 4 km. Image provide by Les Britt, RTI, under NASA contract NAS1-99074.*

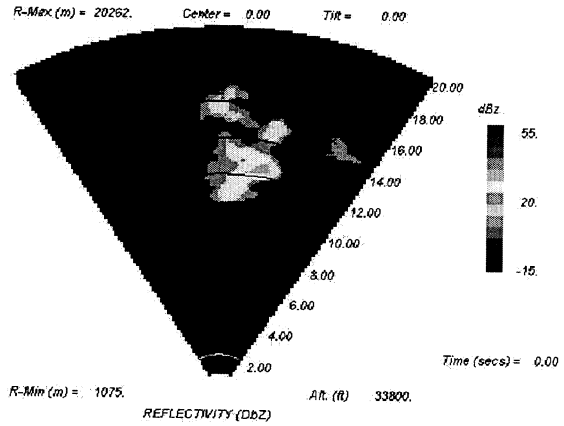

Figure 11. *Radar reflectivity (dBZ) from simulation of onboard radar using TASS data set. Simulation assumes same altitude and heading as in Fig. 10. Range rings every 2 km. Image provide by Les Britt, RTI, under NASA contract NAS1-99074.*

As shown in Fig. 16, the merging of the subgrid extends the inertial subrange to scales less than 50 *m*. The data set is now sufficient to resolve most of the scales important for aircraft response.

A horizontal cross section of the vertical velocity field from the merged data set is shown in Figs. 17. With the addition of the subgrid windfields, the peak updraft and downdraft speeds at flight altitude are 27 *m/s*, and –17 *m/s*, respectively. Significant fluctuations of vertical velocity are confined within regions having some precipitation or cloud material. (cf. Fig. 18).

Hazard Analysis

Using algorithms developed by Bowles, a hazard metric for aircraft turbulence can be applied to the data set. For a particular aircraft, the RMS normal load can be estimated from σ_w using look-up tables;[13] i.e.,

$\sigma_{ng}(x,y) = F\{\sigma_w,$ *altitude, aircraft type, weight, airspeed*$\}$

The σ_w fields can be computed for any horizontal plane in the merged data set, by using a moving average as:

$$\sigma_w(x,y) = \left[\frac{1}{L_x L_y} \int_{x-\frac{L_x}{2}}^{x+\frac{L_x}{2}} \int_{y-\frac{L_y}{2}}^{y+\frac{L_y}{2}} \{w(x',y') - \overline{w}(x,y)\}^2 \, dx'dy' \right]^{\frac{1}{2}}$$

where the averaging interval along the x and y coordinates is L_x, L_y, respectively. The average vertical wind, $\overline{w}$, is computed from the vertical wind, *w, as:*

$$\overline{w}(x,y) = \frac{1}{L_x L_y} \int_{x-\frac{L_x}{2}}^{x+\frac{L_x}{2}} \int_{y-\frac{L_y}{2}}^{y+\frac{L_y}{2}} w(x',y')dx'dy'$$

The value for the averaging interval, L_x=L_y = 1000 *m*, is chosen to correspond to a 4-5 *s* averaging period for a commercial jet at cruise speeds. Hence, the second moment of the *w*-field is computed assuming a 1 *x* 1 *km* moving box.

The σ_w field (Fig. 19) computed from *w* in Fig. 17 exhibits a peak value of 8.2 *m/s*.

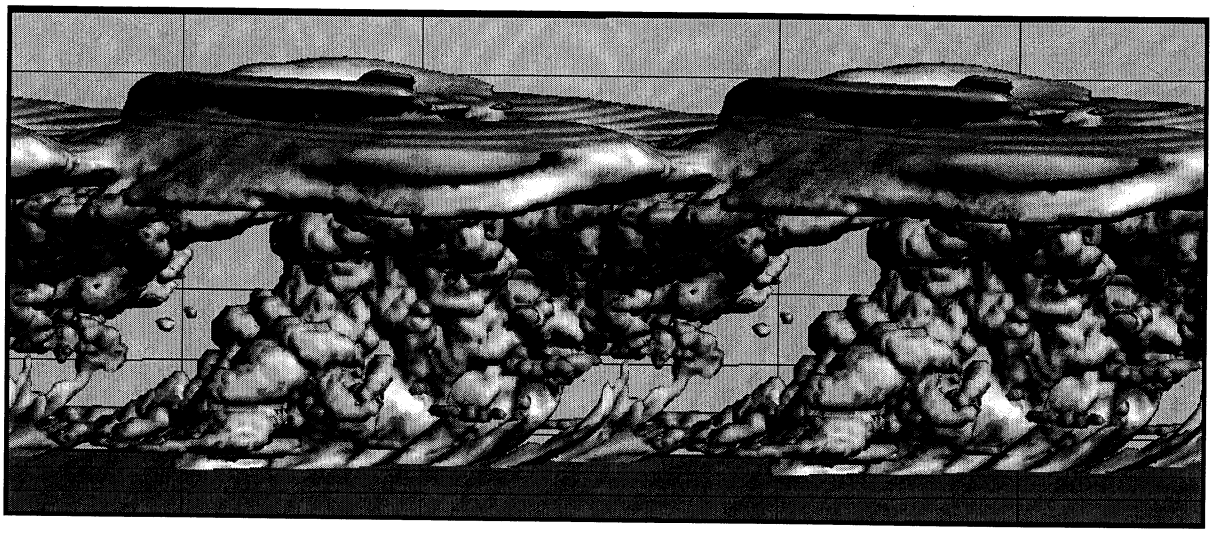

Figure 12. *TASS generated convective-cloud line for event 191-6 as viewed from southeast.*

The RMS normal load (σ_{ng}) is computed from the σ_w fields, assuming aircraft parameters for NASA's B-757 (Fig. 20). Since calculations are independent of aircraft heading, evaluation of the turbulence field is relatively simple. Regions with $\sigma_{ng} > 0.3$ *g* represent severe turbulence, while $0.20\ g \leq \sigma_{ng} \leq 0.30\ g$ represent moderate turbulence. The peak value from the data set is 0.37. The relationship of the hazardous regions with the radar reflectivity can be seen by comparing Figs. 18 and 20. Note that moderate intensity of turbulence is sometimes found in regions of very weak radar reflectivity.

Flight Simulation

A one-dimensional profile of vertical velocity (Fig. 21) was extracted along the arrow shown in Fig. 18. The profile has a peak updraft of 24 *m/s* and is surrounded by strong gradients in vertical velocity. The data in Fig. 21 was used as input into a time-domain flight dynamics model. The output from the dynamic model is shown in Fig. 22. The dynamic model gives a peak $\sigma_{ng} = 0.363$ which compares favorably with the peak value of 0.37 shown in Fig. 20. Very close agreement is obtained even though independent methods are used in calculating σ_{ng}. This supports the credibility of the technique described above for computing σ_{ng} from numerical-model data. A comparison of Fig. 22 with the observed profile of σ_{ng} (Fig.1) exhibits interesting similarities, although weaker than the measured $\sigma_{ng} = 0.44$.

Also of interest is the relation between the peak aircraft loads and its RMS value (see Fig. 22). The peak aircraft loads are nearly instantaneous; and individually, would be difficult to detect by look-ahead sensors. In contrast, the σ_{ng} predictions of hazard encompass the regions of strong peak loads, and are broad enough in horizontal scale to be easily detected.

Radar Simulation

Radar simulations using the merged data set are currently underway. A preliminary result of radar spectral width is shown in Fig. 23. Spectral width actually observed during event 191-6 are shown for onboard-turbulence radar and TLH ground-based radar in Figs. 13b and 14b of reference [2]. The peak value in the radar simulation (7 *m/s*) compares favorably with that observed by TLH radar (7 *m/s*) and onboard radar (8-9 *m/s*).

Table. 2. *RMS Normal Load Comparison*

Source	Peak σ_{ng} (*g's*)
In situ	0.44
Onboard Turbulence Radar$^+$	0.37
Ground-Based Doppler Radar$^+$	0.33
Flight Dynamics Simulation	0.36
Model Diagnostic from σ_w field	0.37
Radar Simulation with Model Data	0.33

$^+$*Computed from radar spectrum width (see reference 13)*

RMS Normal Load Comparison

Table 2 shows a comparison between peak RMS normal loads measured near the B-757 flight path with those simulated from the merged data set. Values for

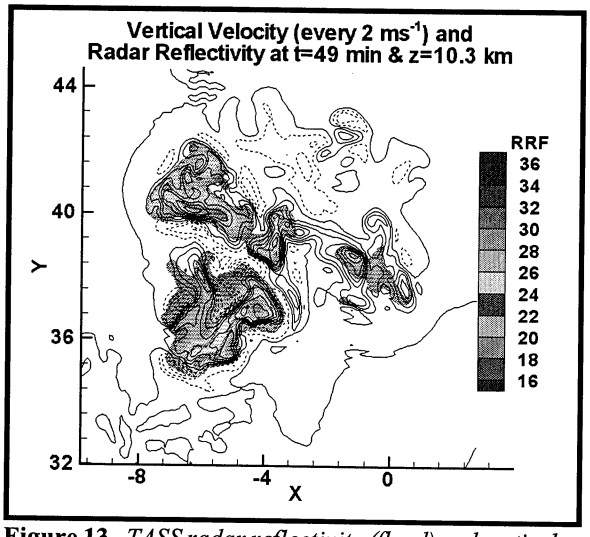

Figure 13. *TASS radar reflectivity (flood) and vertical velocity (2 m/s contours, negative values dashed) along a horizontal cross section at flight level.*

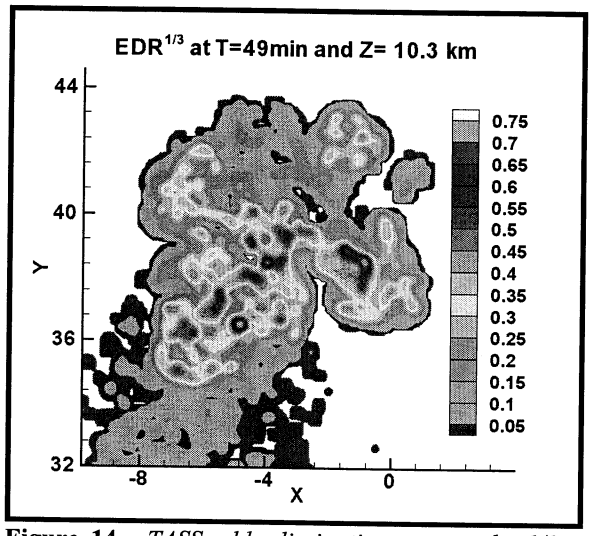

Figure 14. *TASS eddy dissipation rate to the 1/3 power ($m^{2/3}s^{-1}$) at time and location corresponding to Fig. 13.*

σ_{ng} may be obtained from the radar spectrum width by using look-up tables developed by Bowles.[13] All sources indicate a severe turbulence event whether from observed data or simulation.

Summary and Conclusions

A numerical simulation of a convective turbulence event is investigated and compared with observational data. The results have been validated with data from ground based NEXRAD radar, onboard flight radar, and *in situ* measurements. The numerical results show

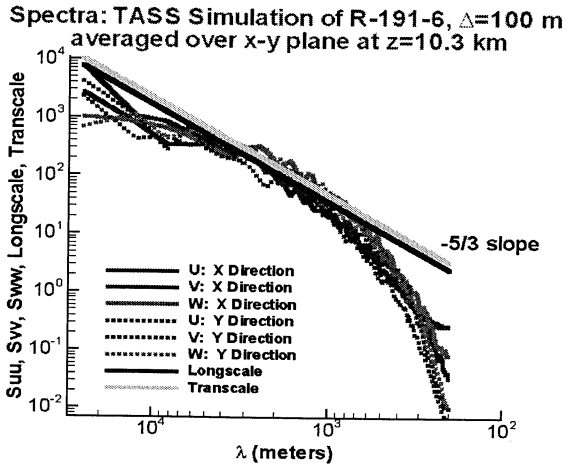

Figure 15. *Energy spectra from TASS, as computed from velocity field within 25x25 km horizontal plain at flight elevation (t=49min).*

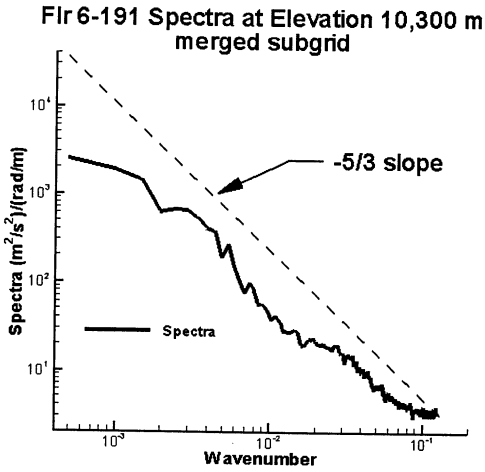

Figure 16. *Energy spectrum from vertical velocity field shown in Fig. 17.*

severe turbulence associated with buoyant plumes that penetrate the upper-level thunderstorm outflow. The peak radar reflectivity in these plumes is 36 *dBZ*. The simulations produce updraft plumes of similar scale to those encountered during the test flight. The simulated radar reflectivity compares well with that obtained from the aircraft's onboard radar.

Resolved scales of motion as small as 50 *m* are needed in order to accurately diagnose aircraft normal load accelerations. Given this requirement, realistic turbulence fields may be created by merging subgrid-scales of turbulence to a convective-cloud simulation.

A hazard algorithm for use with model data sets is demonstrated. The algorithm diagnoses the RMS normal loads from second moments of the vertical velocity field and is independent of aircraft motion.

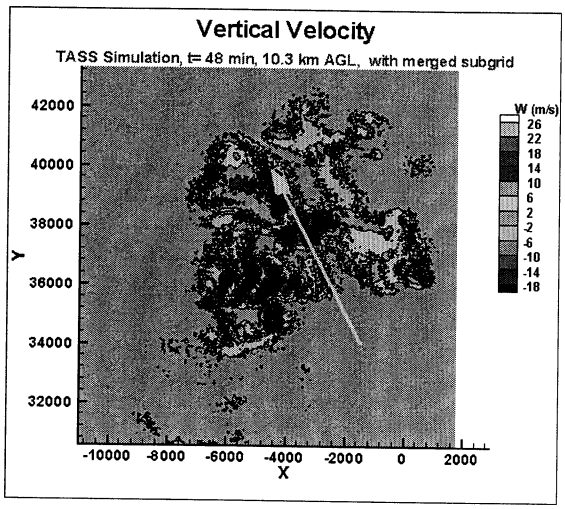

Figure 17. *Vertical velocity field from merged data set. Horizontal cross section at flight altitude (z=10.3 km AGL). [Line shows a hypothetical flight path.]*

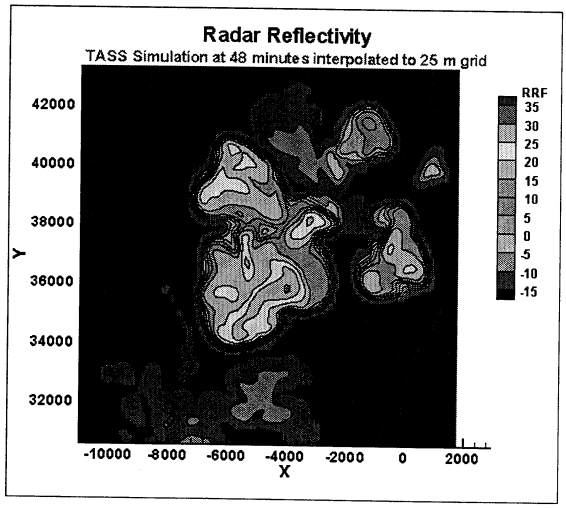

Figure 18. *TASS radar reflectivity field (dBZ) interpolated to domain shown in Fig. 17)*

Acknowledgements

This research was sponsored by NASA's Aviation Safety Program. Numerical simulations were carried out on NASA supercomputers.

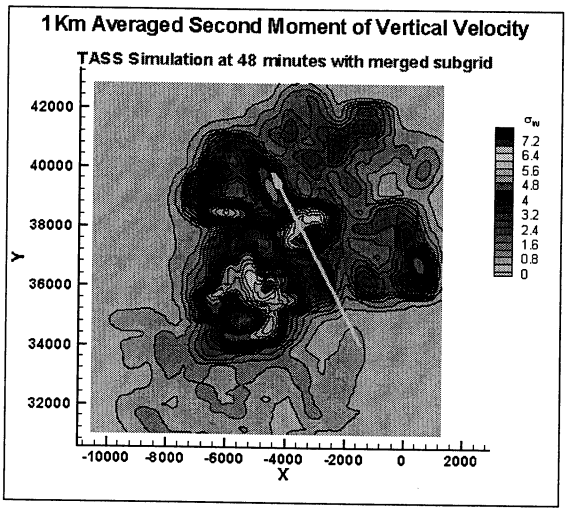

Figure 19. *Diagnosed* σ_w for time and domain shown in Fig. 17.

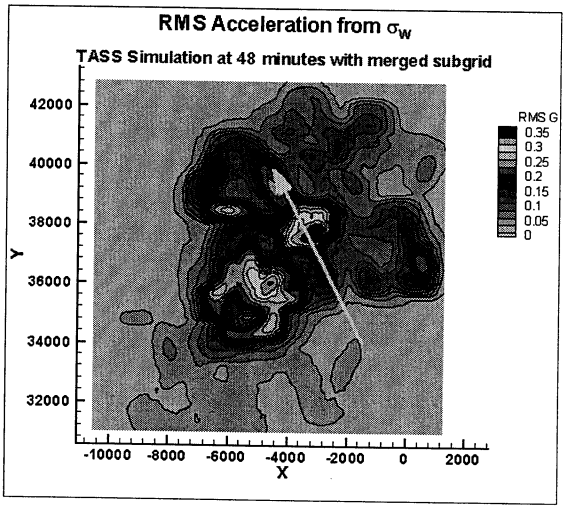

Figure 20. Turbulence hazard field (σ_{ng}) *computed from* σ_w *in Fig. 19.*

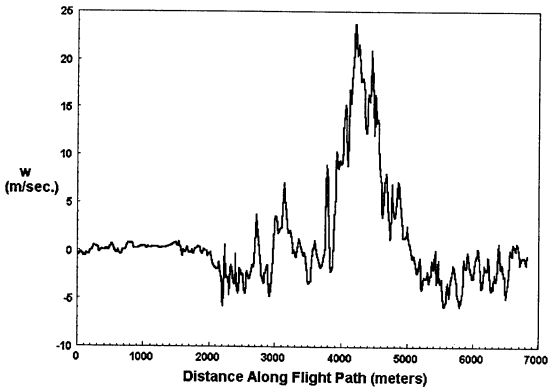

Figure 21. *Vertical velocity field extracted from merged data set along flight path shown in Fig. 17.*

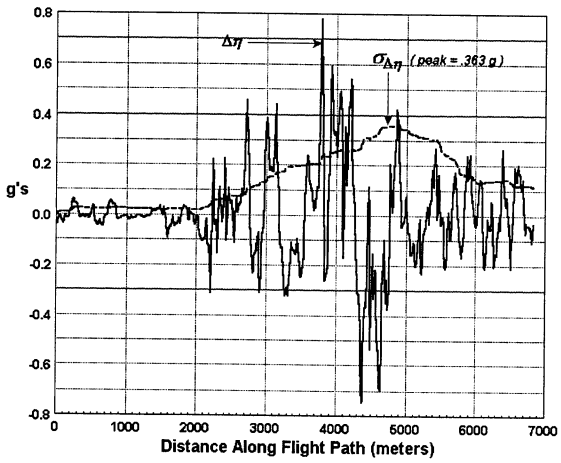

Figure 22. *Normal load acceleration and RMS normal load acceleration (σ_{ng}) vs distance along the flight path as computed from the vertical velocity shown in Fig. 21. Calculation assumes 5 sec moving average (~1 km) and aircraft parameters equivalent to that in 191-6. Local calculations based on 2 degree of freedom B-757 time-domain flight dynamics model.*

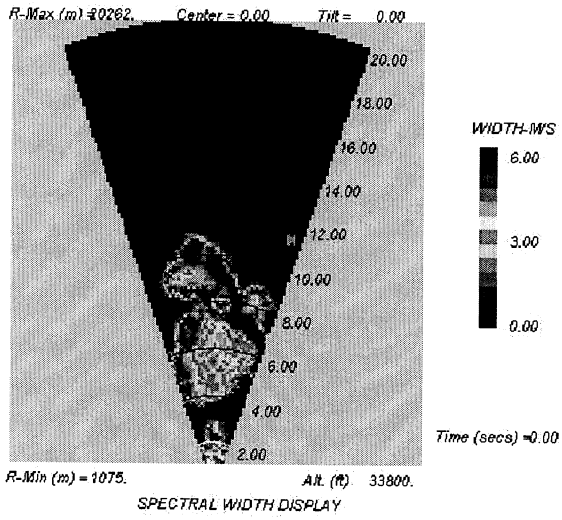

Figure 23 *Spectrum width as simulated with B-757 onboard radar. Range rings every 2 km. Image provide by Carol Kelly, RTI, under NASA contract NAS1-99074.*

References

1. Kaplan, M.L., Lin, Y-L.,Riordan, A.J., Waight, K.T., Lux, K.M, and Huffman, A.W, "Flight Safety Characterization Studies, Part I: Turbulence Categorization Analyses," Interim Subcontrator Report to Research Triangle Institute, NASA contract NAS1-99074, October 1999.

2. Hamilton, D.W., and Proctor, F.H., "Meteorology Associated with Turbulence Encounters During NASA's Fall-2000 Flight Experiments," 40th Aerospace Sciences Meeting and Exhibit, AIAA-2002-0943, 14-17 January 2002, 11pp.

3. Proctor, F.H., "The Terminal Area Simulation System, Volume 1: Theoretical Formulation," NASA Contractor Report 4046, DOT/FAA/PM-85/50, 1, April 1987, 176 pp.

4. Proctor, F.H., "Numerical Simulation of Wake Vortices During the Idaho Falls and Memphis Field Programs," 14th AIAA Applied Aerodynamics Conference, Proceedings, Part-II, New Orleans, LA, AIAA-96-2496, June 1996, pp. 943-960.

5. Proctor, F.H., "Numerical Simulation of Wake Vortices Measured During the Idaho Falls and Memphis Field Programs," 14th AIAA Applied Aerodynamics Conference, Proceedings, Part-II, New Orleans, LA, AIAA Paper No. 96-2496, June 1996, pp. 943-960.

6. DeCroix, D.S., "Large-Eddy Simulations of The Convective and Evening Transition Planetary Boundary Layers," Ph.D. Dissertation, North Carolina State University, Raleigh, N.C., May 2001, 275 pp.

7. Leonard, B.P., "A Stable and Accurate Convective Modelling Procedure Based on Quadratic Upstream Interpolation," *Comp. Meth. Appl. Mech. Eng.*, Vol. 19, 1979, pp. 59-98.

8. Haltiner, G.J. and Williams, R.T., *Numerical Prediction and Dynamic Meteorology,* Second Edition, John Wiley & Sons, 1980, pp. 226-230.

9. Switzer, G.F., "Validation Tests of TASS for Application to 3-D Vortex Simulations," NASA Contractor Report No. 4756, October 1996, 11 pp.

10. Proctor, F.H., and Han, J., "Numerical Study of Wake Vortex Interaction with the Ground Using the Terminal Area Simulation System," 37th Aerospace Sciences Meeting & Exhibit, AIAA-99-0754, January 1999, 12 pp.

11. Kaplan, M.L., Lin, Y-L., Charney, J.J., Pfeiffer, K.D., DeCroix, D.S., and Weglarz, R.P., "A Terminal Area PBL Prediction System at Dallas-Fort Worth and its Application in Simulating Diurnal PBL Jets," *Bull. Amer. Meteor. Soc.,* Vol. 81, 2000, pp. 2179-2204.

12. Bowles, R.L., "Theoretical Investigation of the Relationship between Airborne Radar Observables and Turbulence Induced Aircraft G-loads," AeroTech Report ATR-12007, (prepared for NASA Langley Research Center), October 1999.

13. Bowles, R.L., "Aircraft Centered Hazard Metric Based on Airborne Radar Turbulence Observables," AeroTech Report ATR-12010, (prepared for NASA Langley Research Center), September 2000.

14. Frehlich, R.G., Cornman, L., and Sharman, R., "Simulation of Three-Dimensional Turbulent Velocity Fields," J. Applied Meteor., 40, 2001, pp. 246-258

15. Moeng, C. –H., "A Large Eddy Simulation Model for the Study of Planetary Boundary Layer Turbulence," *Journal of the Atmospheric Sciences*, Vol. 41, 1984, pp. 2052-2062.

16. Schmidt, H., and Schumann, U., "Coherent Structure of the Convective Boundary Layer Derived from Large Eddy Simulations," *Journal of Fluid Mechanics*, Vol. 200, 1989, pp. 212-248.

17. Moeng, C.–H. and Wyngaard, J.C., "Spectral Analysis of Large-Eddy Simulations of the Convective Boundary Layer," *Journal of the Atmospheric Sciences*, Vol. 45, 1988, pp. 3573-3587.

18. Sharman, R., "191-6 Merged Subgrid Turbulence for t=48 min," deliverable to NASA from NCAR under NASA Contract, September 2001.